Highly improved visible-light-driven photocatalytic reduction of Cr (VI) over heterostructured CdS/Bi_2MoO_6 nanocomposite

TINGTING WU, SHANSHAN LIU, FANGFANG, CHENGCAI HUANG, XU ZHANG*
Key Laboratory of Photochemical Biomaterials and Energy Storage Materials, Heilongjiang Province and College of Chemistry and Chemical Engineering, Harbin Normal University, Harbin, 150025, PR China

Heterostructured CdS/Bi_2MoO_6 nanocomposite was prepared based on Bi_2MoO_6 framework assembled from nanoflakes through a two-step facile approach. Photocatalytic activity of the as-synthesized product toward Cr (VI) reduction was studied. The heterostructured CdS/Bi_2MoO_6 nanocomposite shows a much higher photocatalytic activity in the reduction of Cr (VI) to Cr (III) than pure Bi_2MoO_6, and the reduction ratio of Cr (VI) can reach 94.6% in 15 min. The superior photocatalytic reduction activity of the heterostructured nanocomposite was ascribed to the enhanced visible light absorption ability and dramatically boosted separation efficiency of charge carriers.

(Received May 22, 2019, accepted February 17, 2020)

Keywords: CdS/Bi_2MoO_6 nanocomposites, Photocatalysis, Visible-light-driven, Cr (VI) reduction

1. Introduction

Chromium (Cr) is a widely spread contaminant produced through industrial processes such as printing, leather tanning, ceramics manufacturing and is frequently found in waste water. Cr (VI) is highly toxic and is easily absorbed by human body and accumulated in human organs, resulting in rhinitis, pharyngitis, liver damage, renal function failure or even cancer [1, 2]. Therefore, removal of high-risk Cr (VI) from waste water or industrial residues is urgent. Among various techniques for the reduction and removal of Cr (VI) in aqueous media [3-5], photocatalytic reduction of Cr (VI) into Cr (III) under visible light is an efficient and economical method, which has attracted wide attention [6]. As a member of the Aurivillius family of layered perovskites, bismuth molybdate (Bi_2MoO_6) features a layered configuration, and consists of $[Bi_2O_2]^{2+}$ layers interleaved with perovskite-like $[MoO_4]^{2-}$ layers [7-9]. In the past decade, Bi_2MoO_6 has aroused extensive interests due to its highly improved photocatalytic activity for efficient degrading organic pollutants under visible light irradiation [10–12]. However, the practical application of pure Bi_2MoO_6 was still limited [13, 14] because individual-phase Bi_2MoO_6 possesses a low visible light utilization efficiency due to its relatively large band gap (2.5 to 2.8 eV) and the high recombination of photo-induced electrons and holes. How to improve the photocatalytic efficiency of Bi_2MoO_6 to meet practical requirements is still a big challenge. Recently, semiconductor-based heterostructures have been investigated intensively since these new kinds of composite materials may afford more excellent properties in many aspects than single structured material, such as photocatalytic properties, electrochemical properties, and so on. Therefore, many heterostructured composites such as $MoSe_2$/CdSe [15], Ag_2O/ZnO [16], ZnO/ZnS [17], Co_3O_4@ MnO_2 [18], Bi_2WO_6/CdS [19], MCo_2O_4@MCo_2S_4@PPy [20], $NiCo_2O_4$@NiWS [21], MnO_2@$NiCo_2O_4$ [22], $NiCo_2O_4$@$NiMo_2S_4$ [23], MnO_2@$NiCo_2O_4$ [24], $CoMoO_4$@$MoZn_{22}$ [25], etc., have been prepared and studied extensively, and they do exhibit enhanced photocatalytic activities or electrochemical performances as expected by the reporters. Inspired by the successful examples mentioned above, the preparation of Bi_2MoO_6-based composite nanomaterials by combining Bi_2MoO_6 and other semiconductor with suitable band gap is becoming a pivotal strategy for improving the photocatalytic performance of Bi_2MoO_6 in practical applications. CdS is a suitable semiconductor because of its wide light response (up to 520 nm or even longer) and high visible-light-driven photocatalytic activity. So far, several CdS decorated Bi_2MoO_6 nanocomposites have been prepared to improve the photocatalytic properties through an efficient charge transfer process and thereby drive efficient photo-reduction and oxidation reactions at spatially separated sites [26-28]. However, disregard of the applications described above, few reports concerning photocatalytic reduction of Cr (VI) on CdS/Bi_2MoO_6 nanocomposites have been published.

In this work, we have prepared heterostructured

CdS/Bi_2MoO_6 photocatalysts based on star-like Bi_2MoO_6 frameworks by a two-step hydrothermal method. The photocatalytic performance of the products was evaluated toward the reduction of Cr (VI) under visible light irradiation (λ > 400 nm). The results show that the photocatalytic activity of the heterostructured CdS/Bi_2MoO_6 photocatalyst is significantly enhanced in comparison with that of pure CdS or Bi_2MoO_6. Furthermore, a possible mechanism for the improvement of the photocatalytic activity of CdS/Bi_2MoO_6 was discussed.

2. Experimental

All reagents were of analytical grade and were used as received without further purification.

2.1. Synthesis of Bi_2MoO_6

The synthesis method is similar to that reported by Li et al. [29]. In a typical procedure, $Bi(NO_3)_3 \cdot 5H_2O$ (1.0 mmol) and $Na_2MoO_4 \cdot 2H_2O$ (0.5 mmol) was solved in 15 mL of ethylene glycol under stirring to form a homogeneous transparent solution. Then, 0.3 ml of ethylenediamine was added into the solution and white precipitates formed immediately. After being stirred for another 30 min, the mixture was transferred into a 40 mL Teflon-lined stainless autoclave. The autoclave was subsequently heated at 160°C for 6 h. Then the product was collected, washed thoroughly with distilled water and absolute ethanol, and dried at 60°C under ambient air for 12 h.

2.2. Synthesis of heterostructured CdS/Bi_2MoO_6 nanocomposite

CdS/Bi_2MoO_6 heterostructured nanocomposite was synthesized through a facile immersion-deposition process starting from the obtained star-like Bi_2MoO_6 framework. Firstly, 0.0698g Bi_2MoO_6 and 0.0628g $Cd(CH_3COO)_2 \cdot 2H_2O$ was dispersed into 20 mL of deionized water under continuously stirring for 6h. Afterwards the supernatant was thrown away, and then 30 mL H_2O and 0.03906g thiourea was added into the above system under magnetically stirring for 1 h. The reaction solution was transferred into a 50 mL Teflon-lined stainless autoclave. Subsequently the autoclave was heated at 150°C for 15 h. Then the product was collected, washed thoroughly with distilled water and absolute ethanol, and dried at 60°C in vacuum for 12 h.

Pure CdS sample was also prepared by the same procedure in the absence of Bi_2MoO_6.

2.3. Characterization

X-ray powder diffraction (XRD) technique was used to identify the phase composition and crystal structure of the samples. Diffraction data were collected on a Rigaku Dmax-2600/pc diffractometer with Cu Kα radiation (1.542Å). The 2θ scanning range was from 10° to 90° with a scanning speed of 0.15°/s in the continuous mode. Scanning electron microscopy (SEM, Hitachi SU-70 and S4800) was used to observe particle sizes and morphologies of the samples. The element composition and distribution were examined by a SEM equipped with an energy dispersive spectrometer (EDS, EDAX-TEAM Octane Plus). UV–Vis diffuse reflectance spectrum (DRS) data of the samples were collected on a UV-2550 UV–Vis spectrometer (Shimadzu) by using $BaSO_4$ as the reference standard.

2.4. Evaluation of the photocatalytic activity

Catalyst (0.005 g) was added into an aqueous solution (40 mL) containing Cr (VI) ions (50 ppm). The suspension was stirred for 30 min in the dark to attain a balance between adsorption and desorption for the catalyst and Cr (VI). A volume of 4.0 mL of methanol was added as the hole scavenger and the pH value of the suspension was adjusted to 3 with 0.05 N H_2SO_4 solution. The suspension was then irradiated by using a 300W Xe lamp equipped with a cut-off filter (λ>400 nm) under continuous stirring. The distance between xenon lamp and the surface of reaction solution is 20 cm. 1 mL of suspension was sucked out at regular intervals and then was centrifuged immediately. Then the supernatant solution was diluted to 4 mL using deionized water. The absorbance of the diluted sample solution was monitored by using a UV–vis spectrophotometer to determine the concentration of Cr (VI), based on which the photocatalytic activity of the catalyst was measured.

3. Results and discussions

3.1. Phase structure and morphology

Fig. 1 shows the XRD patterns of all of the samples. All of the diffraction peaks in Fig. 1a can be indexed to the hexagonal CdS (JCPDS No. 80-0006). All of the diffraction peaks in Fig. 1b can be indexed to the orthorhombic phase of Bi_2MoO_6 and coincide with the reported data (JCPDS No. 76-2388). The diffraction peaks at 2θ values of 26.51°, 28.04°, 43.96° and 52.13° in Fig. 1c correspond to (002), (101), (110) and (112) planes of hexagonal CdS, respectively. These peaks unambiguously indicate the presence of CdS on the nanocomposite. The other diffraction peaks at 2θ values of 28.33°, 32.46°, 46.98°, 55.50° and 58.52° in Fig. 1c can be indexed to (131), (200), (202), (133) and (262) planes of

orthorhombic Bi_2MoO_6, respectively. In the diffraction pattern of the CdS/Bi_2MoO_6 composite, both CdS and Bi_2MoO_6 were identified, no impurity was observed, indicating the high purity and crystallization of the product and the synthesized composite material possesses a two-phase composition.

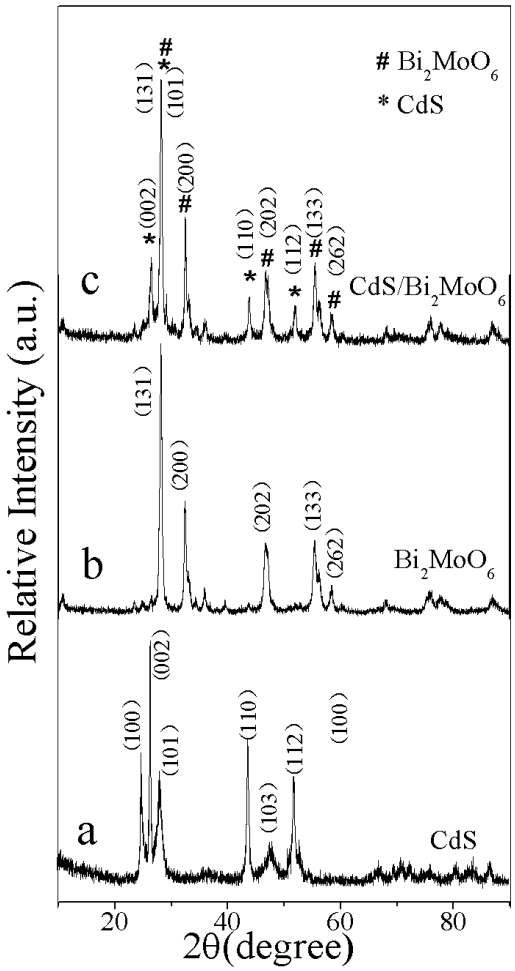

Fig. 1. XRD patterns of the as-synthesized samples

Fig. 2 is SEM images of the samples. Fig. 2a is a typical SEM image of pristine Bi_2MoO_6. It shows that the product is composed of many uniform star-like microstructures with a diameter of ~1 μm. And the star-like microstructure is constructed by some inter-crossed nanoflakes with an average thickness of ~30 nm. Fig. 2b shows an enlarged SEM image of CdS/Bi_2MoO_6 nanocomposite which clearly displays that the outline is similar to that of pure Bi_2MoO_6. It can be seen that the interspaces of Bi_2MoO_6 coming from the intercrossed nanoflakes have been filled by irregular CdS nanoparticles, resulting in intimate contact between CdS and Bi_2MoO_6, which was believed to facilitate the transfer of photogenerated charges.

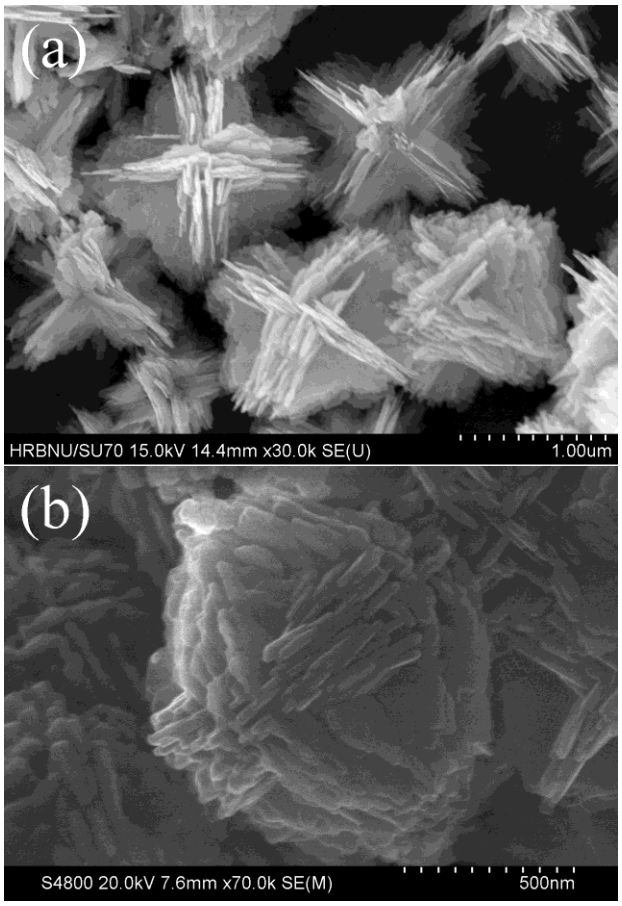

Fig. 2. SEM images of pristine Bi_2MoO_6 (a) and heterostructured CdS/Bi_2MoO_6 nanocomposite (b)

3.2. Elemental composition analysis

In order to demonstrate the successful fabrication of CdS/Bi_2MoO_6 heterostructure, EDS analysis was also employed to test and verify the real existence and uniform distribution of CdS nanoparticles in CdS/Bi_2MoO_6 heterostructures. The presence of Mo, Bi, O, S, and Cd elements in the composite can be proved evidently by the EDS elemental spectrum of CdS/Bi_2MoO_6 (Fig. 3b). The EDS elemental mapping of the CdS/Bi_2MoO_6 composite (Fig. 3c–h) displays that Cd element and S element are distributed uniformly on the surface of the star-like Bi_2MoO_6 framework. The elements of Cd and S are from CdS. The results further indicate that the CdS nanocrystals have been successfully and firmly grown on the surface of the Bi_2MoO_6.

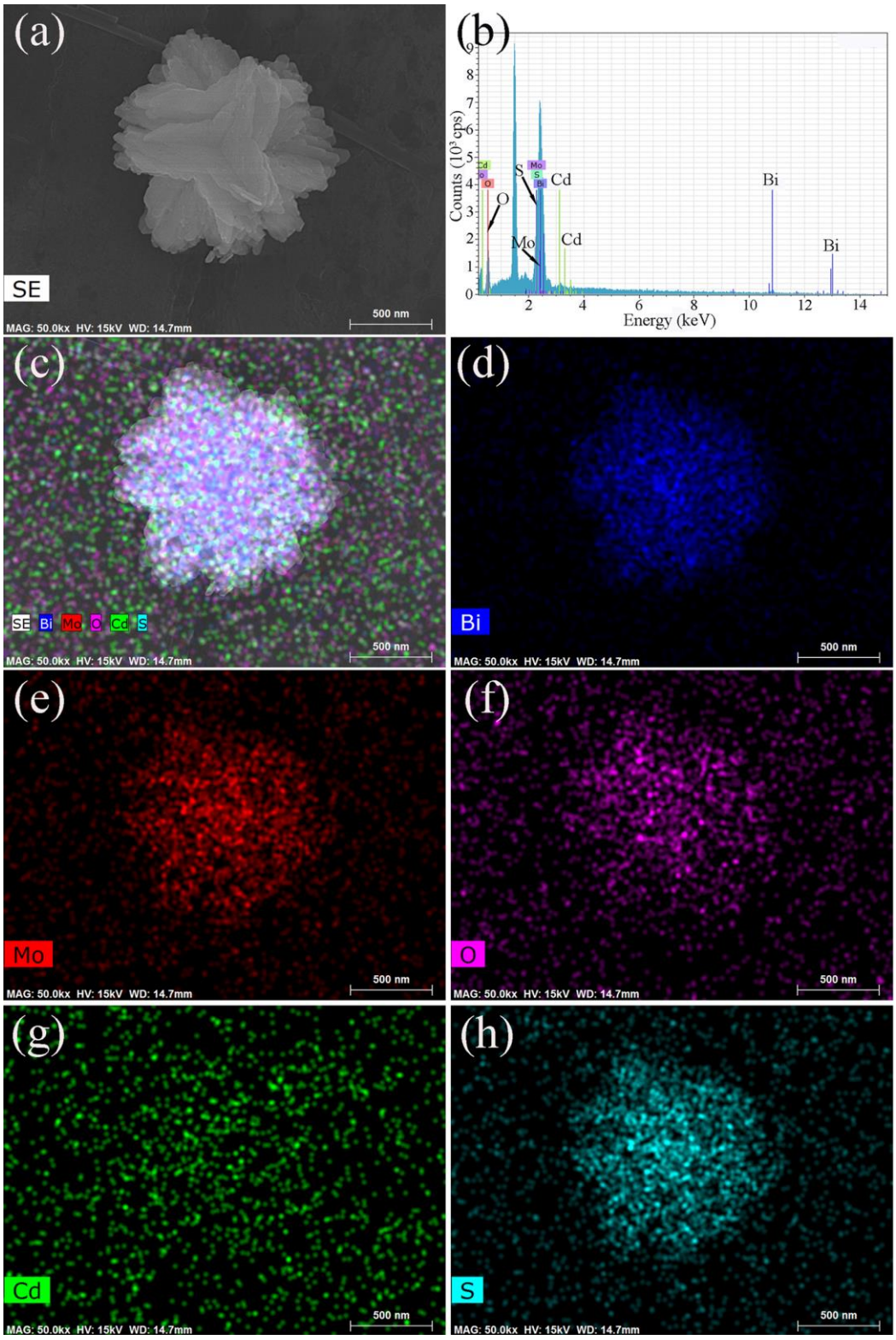

Fig. 3. (a) SEM image of a single CdS/Bi_2MoO_6 heterostructured nanocomposite; (b) EDS elemental spectrum of the as-prepared CdS/Bi_2MoO_6 nanocomposite; (c) EDS mapping of all elements in the CdS/Bi_2MoO_6 nanocomposite; maps of the distribution of each element: (d) Bi element, (e) Mo element, (f) O element, (g) Cd element and (h) S element (color online)

3.3. UV-Vis diffusion reflectance spectra

The DRS was employed to study the photo-responsive performance of the samples and the results are shown in Fig. 4a. Pure Bi_2MoO_6 exhibits strong photoresponse from ultraviolet region to visible light region and the absorption edge is around 506 nm. The absorption edge of CdS/Bi_2MoO_6 shows an obvious red-shift in visible light

region compared to pure Bi_2MoO_6, indicating a decreased band gap energy. The band gap values of the prepared samples are estimated by the formula as follow:

$$(\alpha hv)^n = C(hv - E_g) \quad (1)$$

where E_g is band gap energy, h is Planck constant, α is the absorption coefficient, v and C are light frequency and constant, respectively. Here, n is 2 for Bi_2MoO_6, CdS and CdS/Bi_2MoO_6. As a result, the approximate band gap energies of the samples are ~2.77 eV for pristine Bi_2MoO_6, ~2.17eV for pristine CdS and ~2.21 eV for CdS/Bi_2MoO_6, respectively (Fig. 4b).

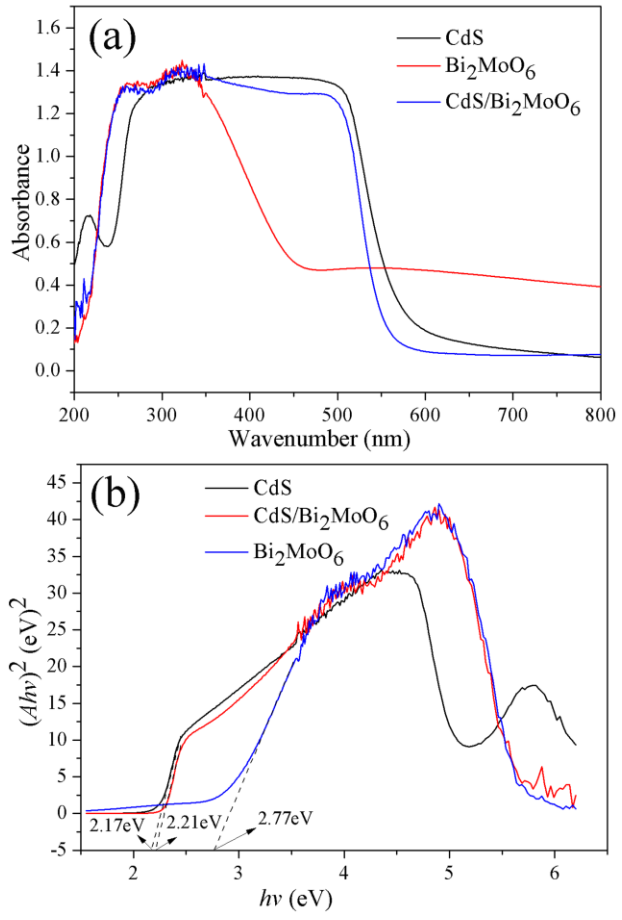

Fig. 4. (a) UV–Vis absorption spectra of Bi_2MoO_6, CdS, and CdS/Bi_2MoO_6; (b) Kubelka–Munk plot for band gap calculation of Bi_2MoO_6, CdS, and CdS/Bi_2MoO_6 (color online)

Considering that the band edge positions of conduction band (CB) and valence band (VB) in photocatalyst play an important role in the photocatalytic activity, the CB and VB potentials of the semiconductor at the point of zero charge can be calculated by the following equation:

$$E_{CB} = X + E_0 - 0.5E_g \quad (2)$$

$$E_{VB} = E_{CB} + E_g \quad (3)$$

where E_g represents the band gap energy of the semiconductor, E_{CB} and E_{VB} are the conduction band edge and valence band edge of a semiconductor at the point of zero charge, respectively, E_0 is the energy of free electrons on the hydrogen scale (− 4.5 eV), and X is the absolute electronegativity of the semiconductor, expressed as the geometric mean of the absolute electronegativity of the constituent atoms, which is defined as the arithmetic mean of the atomic electron affinity and the first ionization energy. The E_{CB} and E_{VB} of pure Bi_2MoO_6 are calculated to be 0.425 and 3.195 eV, respectively. For CdS nanoparticles, both the values of E_{CB} (− 0.395 eV) and E_{VB} (1.775 eV) are lower than the corresponding values of Bi_2MoO_6, indicating that the type-II band gap alignment could be fabricated. Particularly, the difference of chemical potential between semiconductor Bi_2MoO_6 and CdS can cause band bending at the interface of junction. The band bending induces a built-in field, which drives the photogenerated electrons and holes to move in opposite directions, leading to a spatial separation of the electrons and holes on different sides of heterojunction [30]. Thus, the fabrication of CdS/Bi_2MoO_6 heterojunction will be in favor of the improvement of photocatalytic activity.

3.4. Photocatalytic activity of samples

The photocatalytic activity of the as-prepared samples was evaluated through the reduction of Cr (VI) to water insoluble Cr (III) under visible light irradiation. Figure 5a shows the photoreduction curves of Cr (VI) in the presence of different catalyst after irradiation for different times at ambient conditions, where C_0 is the equilibrium concentration of Cr (VI) in the dark, and C_t is the concentrations of Cr (VI) in solution at desired time. It can be seen that about 47.8% of Cr (VI) is reduced by pure Bi_2MoO_6 frameworks after 100 min light irradiation and about 91.4% of Cr (VI) is reduced by pure CdS after 30 min light irradiation. Notably, the heterostructured CdS/Bi_2MoO_6 nanocomposite exhibits the superior reduction performance that about 94.6% of Cr (VI) is reduced after 15 min light irradiation, which could be attributed to the effective interfacial charge transfer resulted from the fabricated heterojunctions between Bi_2MoO_6 and CdS. However, blank test without any catalyst exhibits a photoreduction degree of 6.4% in 15 min and 36.5% in 100 min, which suggests a contribution of methanol to the Cr (VI) reduction reaction even in the absence of catalysts. In view of rapid reaction rate of the

CdS/Bi_2MoO_6 heterostructure for the Cr (VI) reduction, the effect of methanol on the Cr (VI) reduction is negligible.

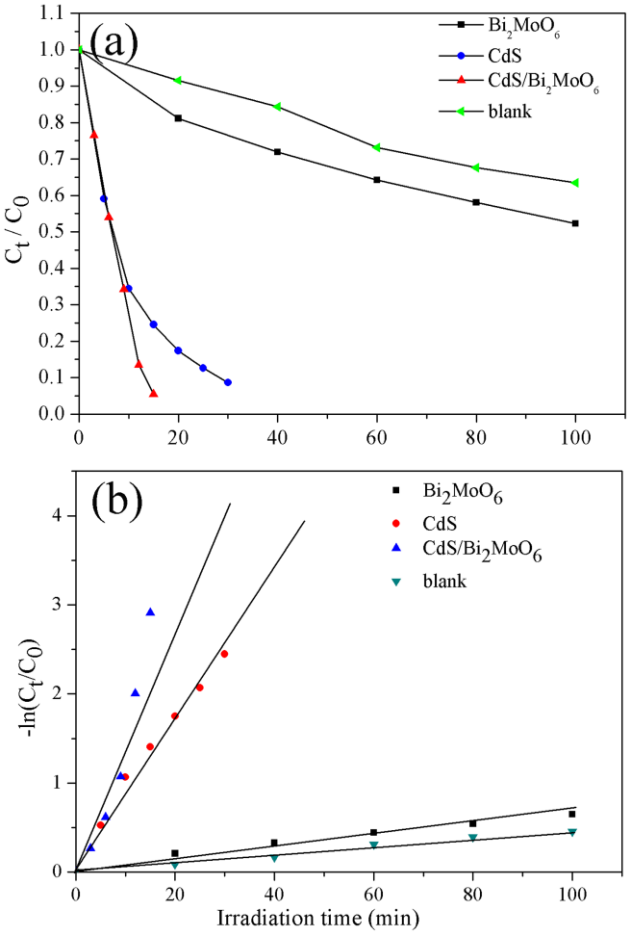

Fig. 5. Photoreduction of Cr(VI) at different time intervals under visible light irradiation. (a) C_t/C_0 concentration changes of Cr(VI) as a function of time using different catalysts; (b) Logarithmic concentration ratio of the samples as a function of time for photoreduction of Cr(VI) solution (color online)

To make a quantitative comparison, the Cr (VI) reduction data were fitted with the following pseudo-first-order model [31] (Fig. 5b)

$$-\ln(C_t/C_0) = kt \quad (4)$$

Clearly, CdS/Bi_2MoO_6 shows the largest rate constant of 0.1431 min^{-1}, which is approximately 1.6 and 19.4 times higher than pristine CdS (0.08752 min^{-1}) and Bi_2MoO_6 (0.007381 min^{-1}).

3.5. Proposed photo-reduction mechanism over CdS/Bi_2MoO_6 photocatalyst

On the basis of the above band energy level analysis, the possible photocatalytic mechanism was supposed as illustrated in Fig. 6. When the CdS/Bi_2MoO_6 composite is irradiated by visible light, the photogenerated electron–holes could be produced in the CB and VB of both CdS and Bi_2MoO_6, respectively. As the CB level of CdS is more negative than that of Bi_2MoO_6, the photogenerated electrons in the CB of CdS are easy to migrate to the CB of Bi_2MoO_6, at the same time the holes in the VB of Bi_2MoO_6 can transfer to the VB of CdS. Due to the strong interfacial interaction between Bi_2MoO_6 and CdS, the photogenerated electrons and holes in Bi_2MoO_6 and CdS are effectively separated. Therefore, the heterostructured CdS/Bi_2MoO_6 nanocomposite exhibits superior photocatalytic performance to pure Bi_2MoO_6. Thus it can be concluded that it is the introducing of CdS that endow the heterostructured CdS/Bi_2MoO_6 nanocomposite an enhanced photocatalytic performance.

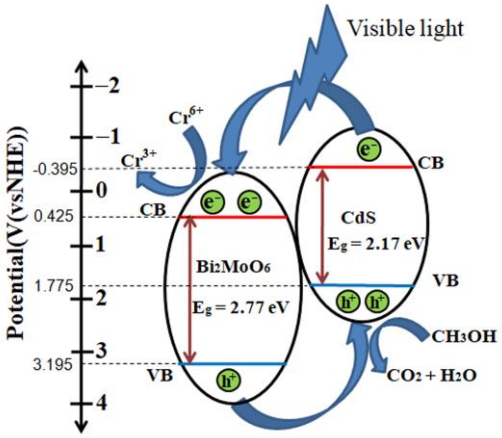

Fig. 6. Schematic illustration of photogenerated electron–hole pairs separation on CdS/Bi_2MoO_6 nanocomposite under visible light irradiation (color online)

4. Conclusions

Heterostructured CdS/Bi_2MoO_6 nanocomposite was synthesized successfully based on star-like Bi_2MoO_6 frameworks composed of inter-crossed nanoflakes. The photoreduction efficiency of the nanocomposite toward Cr (VI) was approximately 1.6 and 19.4 times of pure CdS and Bi_2MoO_6, respectively. The facilitated interfacial charge transfer and decreased electron–hole recombination due to the formation of CdS/Bi_2MoO_6 heterojunctions is believed to be responsible to the enhanced photocatalytic activities of the as-obtained heterostructured CdS/Bi_2MoO_6 nanocomposite. Based on the experimental results, the photocatalytic mechanism on CdS/Bi_2MoO_6 nanocomposite is proposed. The research results clearly indicate that the fabrication of type II heterostructure by coupling semiconductor with narrow band gap is proved to be an effective approach to improve the photocatalytic performance of the Bi_2MoO_6.

Acknowledgement

This work was supported by the Innovative Program of Graduate Student of Harbin Normal University (No. HSDSSCX2018-21).

References

[1] B. A. Marinho, R. O. Cristovao, R. Djellabi, J. M. Loureiro, R. A. R. Boaventura, V. J. P. Vilar, Appl. Catal. B: Environ. **203**, 18 (2017).
[2] R. Wang, G. Cheng, Z. Dai, J. Ding, Y. Liu, R. Chen, Chem. Eng. J. **327**, 371 (2017).
[3] N. M. Dogan, C. Kantar, S. Gulcan, C. J. Dodge, B. C. Yilmaz, M. A. Mazmanci, Environ. Sci. Technol. **45**, 2278 (2011).
[4] J. Wang, K. Pan, Q. He, B. Cao, J. Hazard. Mater. **244–245**(1), 121 (2013).
[5] B. Qiu, C. Xu, D. Sun, H. Yi, J. Guo, X. Zhang, H. Qu, M. Guerrero, X. Wang, ACS Sustainable Chem. Eng. **2**, 2070 (2014).
[6] A. Rauf, S. A. S. Shah, G. H. Choi, U. B. Humayoun, D. H. Yoon, J. W. Bae, J. Park, W. J. Kim, P. J. Yoo, ACS Sustainable Chem. Eng. **3**(11), 2847 (2015).
[7] J. Tian, P. Hao, N. Wei, H. Cui, H. Liu, ACS Catal. **5**, 4530 (2015).
[8] J. Lv, K. Dai, J. Zhang, L. Geng, C. Liang, Q. Liu, G. Zhu, C. Chen, Appl. Surf. Sci. **358**, 377 (2015).
[9] J. Di, J. Xia, M. Ji, H. Li, H. Xu, H. Li, R. Chen, Nanoscale **7**, 11433 (2015).
[10] J. H. Bi, L. Wu, J. Li, Z. H. Li, X. X. Wang, X. Z. Fu, Acta Mater. **55**, 4699 (2007).
[11] L. Zhou, W. Z. Wang, L. S. Zhang, J. Mol. Catal. A **268**, 195 (2007).
[12] L. J. Xie, J. F. Ma, G. J. Xu, Mater. Chem. Phys. **110**, 197 (2008).
[13] Y. Shi, S. Feng, C. Cao, Mater. Lett. **44**, 215 (2000).
[14] M. Shang, W. Wang, J. Ren, S. Sun, L. Zhang, Nanoscale **3**, 1474 (2011).
[15] Y. Wang, J. X. Zhao, Z. Chen, F. Zhang, W. Guo, H. M. Lin, F. Y. Qu, Appl. Catal. B: Environ. **244**, 76 (2019).
[16] J. Wang, F. Y. Qu, X. Wu, Sci. Adv. Mater. **5**, 1364 (2013).
[17] W. N. Jia, B. X. Jia, F. Y. Qu, X. Wu, Dalton Trans. **42**, 14178 (2013).
[18] X. Zheng, Z. C. Han, W. J. Yang, F. Y. Qu, B. D. Liu, X. Wu, Dalton Trans. **45**, 16850 (2016).
[19] Y. F. Liu, S. S. Liu, T. T. Wu, H. M. Lin, X. Zhang, J Sol-Gel Sci. Technol. **83**, 315 (2017).
[20] D. P. Zhao, H. Q. Liu, X. Wu, Nano Energy **57**, 363 (2019).
[21] D. P. Zhao, M. Z. Dai, H. Q. Liu, L. Xiao, X. Wu, H. Xia, Cryst. Growth Des. **19**, 1921(2019).
[22] D. P. Zhao, M. Z. Dai, Y. L. Tong, X. F. Song, X. Wu, CrystEngComm **21**, 5789 (2019).
[23] D. P. Zhao, M. Z. Dai, H. Q. Liu, K. F. Chen, X. F. Zhu, D. F. Xue, X. Wu, J. P. Liu, Adv. Mater. Interfaces **6**, 1901308 (2019).
[24] D. P. Zhao, X. Wu, C. F. Guo, Inorg. Chem. Front. **5**, 1378 (2018).
[25] H. Q. Liu, D. P. Zhao, Y. Liu, P. F. Hu, X. Wu, H. Xia, Chem. Eng. J. **373**, 485(2019).
[26] Y. Feng, X. Yan, C. B. Liu, Y. Z. Hong, L. Zhu, M. J. Zhou, W. D. Shi, Appl. Sur. Sci. **353**, 87 (2015).
[27] H. Yang, Z. L. Jin, H. Y. Hu, G. X. Lu, Y. P. Bi, RSC Adv. **7**, 10774 (2017).
[28] S. J. Li, Y. P. Liu, Y. Q. Long, L. Y. Mo, Catalysts **8**, 477 (2018).
[29] Z. Q. Li, X. T. Chen, Z. L. Xue, CrystEngComm, **15**, 498 (2013).
[30] H. McDaniel, P. E. Heil, C. L. Tsai, K. K. Kim, M. Shim, ACS Nano **5**, 7677 (2011).
[31] V. A. Sakkas, I. M. Arabatzis, I. K. Konstantinou, A. D. Dimou, T. A. Albanis, P. Falaras, Appl. Catal. B: Environ. **49**, 195 (2004).

*Corresponding author: xzhang@hrbnu.edu.cn